

**Emergent oscillations in unidirectionally coupled overdamped bistable systems**Adi R. Bulsara,<sup>1,\*</sup> Visarath In,<sup>1,†</sup> Andy Kho,<sup>1,‡</sup> Patrick Longhini,<sup>2,§</sup> Antonio Palacios,<sup>2,||</sup> Wouter-Jan Rappel,<sup>3,¶</sup>  
Juan Acebron,<sup>4,\*\*</sup> Salvatore Baglio,<sup>5,††</sup> and Bruno Ando<sup>5,‡‡</sup><sup>1</sup>Space and Naval Warfare Systems Center, Code 2363, 53560 Hull Street, San Diego, California 92152-5001, USA<sup>2</sup>Nonlinear Dynamics Group, Department of Mathematics & Statistics, San Diego State University, San Diego, California 92182, USA<sup>3</sup>Physics Department, University of California at San Diego, La Jolla, California 92093, USA<sup>4</sup>Dipartimento di Ingegneria dell' Informazione, Università di Padova, Via Gradenigo 6/B, 35131 Padova, Italy<sup>5</sup>Dipartimento di Ingegneria Elettrica Elettronica e dei Sistemi, Università degli Studi di Catania,  
Viale A. Doria 6, 95125 Catania, Italy

(Received 12 February 2004; published 3 September 2004)

It is well known that overdamped unforced dynamical systems do not oscillate. However, well-designed coupling schemes, together with the appropriate choice of initial conditions, can induce oscillations when a control parameter exceeds a threshold value. In a recent publication [Phys. Rev. E, **68**, 045102(R) (2003)], we demonstrated this behavior in a specific prototype system, a soft-potential mean-field description of the dynamics in a hysteretic “single-domain” ferromagnetic sample. The previous analysis of this work showed that  $N$  (odd) unidirectionally coupled elements with cyclic boundary conditions would, in fact, oscillate when a control parameter—in this case the coupling strength—exceeded a critical value. These oscillations are now finding utility in the detection of very weak “target” signals, via their effect on the oscillation characteristics, e.g., the frequency and asymmetry of the oscillation wave forms. In this paper we explore the underlying dynamics of this system. Scaling laws that govern the oscillation frequency in the vicinity of the critical point, as well as the zero-crossing intervals in the presence of a symmetry-breaking target dc signal, are derived; these quantities are germane to signal detection and analysis.

DOI: 10.1103/PhysRevE.70.036103

PACS number(s): 02.50.Ey, 05.10.Gg, 05.40.–a

**I. INTRODUCTION**

Overdamped bistable dynamics, of the generic form  $\dot{x} = -\nabla U(x)$  underpin the behavior of numerous systems in the physical world. The most studied example is the overdamped Duffing system: the dynamics of a particle in a bistable potential  $U(x) = -ax^2 + bx^4$ . Frequently, bistable systems are also characterized by a “soft” potential (to be contrasted with the “hard” Duffing potential which approaches  $\pm\infty$  far more steeply) consisting of a nonlinear addition to a parabolic component, the latter being, of course, characteristic of linear dynamics. Among these systems, the dynamics of a hysteretic ferromagnetic core (treated as a macroscopic single-domain entity) have recently attracted some attention, because they underpin very inexpensive magnetic field sensors, operated in the time domain [2]. Absent an external forcing term, the state point  $x(t)$  will rapidly relax to one of two stable attractors, for any choice of initial condition. This behavior is, of course, universal in overdamped dynamical systems.

In two recent papers [1,3], we have demonstrated that coupling an *odd* number  $N \geq 3$  of overdamped bistable elements in a ring, with unidirectional coupling, and ensuring that at least one of them has an initial state that is different from the others, can lead to oscillatory behavior when the coupling strength exceeds a critical value. The characteristics of the bifurcation to oscillatory behavior depend on the system dynamics and, more importantly, the manner in which the elements are coupled. For the case of Duffing dynamics with additive inter-element coupling [3], the system undergoes a Hopf bifurcation to oscillatory behavior; the oscillation frequency is nonzero infinitesimally past the bifurcation point, and increases as one goes deeper into the bifurcation regime. In [3], this property was exploited in a simple model of two interacting neural “columns,” and shown to lead to the appearance of certain well-characterizable frequency components in the response. In [1], we considered a system of coupled elements having “soft”-potential dynamics, characteristic of hysteretic single-domain ferromagnetic cores. This work has led to exploiting the emergent oscillatory behavior for signal detection purposes: specifically, an external symmetry-breaking dc magnetic signal having small amplitude (usually much smaller than the energy barrier height of a single element) can be detected and quantified via its effect on the oscillation frequency and asymmetry of the oscillation wave forms. For this case, the continuum limit of a discrete (spin system) representation [6] dictates the nature of the coupling (somewhat more complicated than the additive coupling used in the Duffing system). The bifurcation to *observable* oscillatory behavior for this case is not Hopf; rather it occurs through the confluence of heteroclinic cycles, and displays some properties reminiscent of a saddle-node bifurca-

\*Electronic address: bulsara@spawar.navy.mil

†Electronic address: visarath@spawar.navy.mil

‡Electronic address: kho@spawar.navy.mil

§Electronic address: plonghini@netzero.net

||Electronic address: palacios@euler.sdsu.edu

¶Electronic address: rappel@physics.ucsd.edu

\*\*Electronic address: acebron@dei.unipd.it

††Electronic address: salvatore.baglio@diees.unict.it

‡‡Electronic address: bruno.ando@diees.unict.it

tion (e.g., the oscillation frequency is zero at the critical point). We reiterate that the above-outlined behavior occurs only for an odd number of elements  $N \geq 3$  (the analogy to a frustrated spin system comes to mind, and this analogy will become increasingly transparent as we proceed through our treatment of the dynamics just past the critical point), with cyclic unidirectional coupling and initial conditions selected so that at least one state point is different from the others.

In this work, we proceed as follows. In Sec. II, we present a brief overview of emergent oscillations in coupled Duffing oscillators. This section is included for nonspecialists; readers familiar with the mechanisms of coupling-induced oscillations might want to skip it. In Sec. III we reconsider the dynamics of unidirectionally coupled single-domain ferromagnetic cores, with a view to substantially enhancing our earlier results [1]. We report results of the bifurcation analysis for a model of  $N$  fluxgate magnetometers unidirectionally coupled in a ring. The analysis includes an extension of the  $N=3$  case, which was introduced in [1], to larger values of  $N$ . In particular, we conclude that if the coupling scheme is unidirectional among nearest neighbors then coupling-induced oscillations are possible only when  $N$  is odd. In Sec. IV we use a simplified two-state model to get insight into the coupled system dynamics. In spite of the simplifications, the two-state model captures essential features of the original system that explain the nature of the oscillations and why they are found only when  $N$  is odd. In Sec. V, we discuss in more detail the behavior of the coupled system near the critical point where oscillations occur. We demonstrate how one can derive the oscillation frequency together with its scaling behavior as a function of the coupling strength, which is considered to be our control parameter. This frequency, and the zero crossings of the response, serve as useful quantifiers of a very small (compared to the hysteresis loop width) “target” signal, assumed to be dc throughout this work. As already mentioned, this system and its unique (mean-field) coupling are germane to the design of inexpensive fluxgate magnetometers, operated in the time domain. In Sec. VI we describe an experimental setup involving three coupled fluxgates. More importantly, we show that the theoretical results of this paper complement the experimental work very well.

The results of this paper and our earlier work [1] are already being applied to the design of arrays of fluxgate magnetic field sensors which afford the possibilities of low onboard power, as well as the ability to operate in the regime (just past the critical point) of maximal sensitivity if one can develop a technique for “tuning” the control parameter, in this case the coupling strength, in response to changes in the target field in real operational scenarios. We do not address many of these practical issues here; rather, we limit ourselves to a description of the dynamics, especially close to the onset of the bifurcation from static to oscillating behavior. In this regime, the dynamics are particularly sensitive to small external signals which render the underlying potential energy function (in the absence of coupling) asymmetric.

## II. EMERGENT OSCILLATIONS IN COUPLED OVERDAMPED DUFFING OSCILLATORS

In this section we describe, briefly, the mechanism for the generation of oscillations in a simpler system of three (uni-

directionally) coupled bistable overdamped Duffing oscillators:

$$\begin{aligned}\dot{x}_1 &= ax_1 - bx_1^3 + \lambda(x_1 - x_2), \\ \dot{x}_2 &= ax_2 - bx_2^3 + \lambda(x_2 - x_3), \\ \dot{x}_3 &= ax_3 - bx_3^3 + \lambda(x_3 - x_1).\end{aligned}\tag{1}$$

The overdamped Duffing system is of interest in its own right; it has been used as a model to provide a qualitative window into systems as diverse as the dynamics of the photon number density in a lasing cavity and single-neuron dynamics. As already mentioned, the dynamics in this system are quite different from those in the coupled magnetic system that comprises the thrust of this paper; this is due to the different coupling mechanism. Our aim, in outlining the mechanism of the emergent oscillations for this case, is to underline the fact that the emergent oscillatory behavior can be seen in a wide class of nonlinear dynamic systems which can have different coupling schemes and potential energy functions. For both systems, much of the bifurcation analysis has already been carried out [1,3], part of it using numerical routines, e.g., AUTO [5], and will not be repeated in this paper.

A fixed point exists where the right-hand sides of the system (1) are zero and it is trivial to find this solution with some algebraic manipulations. Linearizing about this point  $(x_1, x_2, x_3) = (0, 0, 0)$ , we readily obtain the eigenvalues of the ensuing dynamics near the fixed point; they consist of one real eigenvalue together with a complex conjugate pair:  $a + (3/2)\lambda \pm (\sqrt{3}/2)\lambda i$ . Hence, a Hopf bifurcation occurs when the real part vanishes, i.e., at the critical value  $a_c = -(3/2)\lambda$ . The oscillation frequency is simply the imaginary part of the eigenvalues,  $\omega = (\sqrt{3}/2)\lambda$ , which remains approximately constant close to the critical point (the realm of validity of the linearization). Figure 1 shows the oscillatory behavior obtained via direct simulation of (1). The oscillations remain approximately sinusoidal very close to the critical parameter; in this regime, their amplitude can be found by substituting a trial solution of the form  $A \sin \omega t$  into the dynamics, realizing that all the state points oscillate at the same frequency but are offset in phase by  $2\pi/3$ , and retaining only the oscillatory terms at the fundamental frequency  $\omega$ . One then obtains  $A = (2/\sqrt{3}b)\sqrt{a - a_c}$  for the oscillation amplitude. As one goes deeper into the oscillatory regime (by adjusting  $a$  or  $\lambda$ ), the character of the oscillations changes dramatically; the frequency drops, the oscillations lose their sinusoidal character (corresponding to an operating regime wherein the linearized system is no longer applicable), and, for sufficiently large values of the control parameter, they can be suppressed. This behavior, occurring in a regime where analytic calculations may be formidable, is not discussed further.

With the (relatively simple) example of emergent oscillatory behavior in the system (1) as a starting point, we now address the problem at the heart of this paper: a system of coupled (via a mean-field interaction) hysteretic ferromagnetic cores, which underpins the dynamics of simple “fluxgate” magnetometers [2,4].

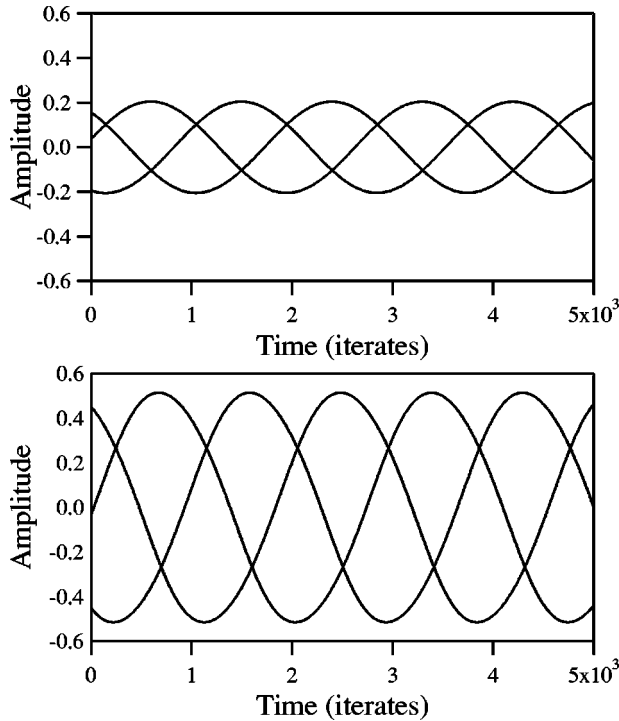


FIG. 1. The coupled Duffing system ( $N=3$ ) has two Hopf bifurcations off the local fixed point  $(0,0,0)$ . One bifurcation is for  $\lambda = 2/3a$  and the other is for  $a = -3/2\lambda$ . The  $\lambda = (2/3)a$  case is unstable and, hence, unobservable. The other case is stable. Top: the coupled Duffing system oscillating for  $a = -1.47, \lambda = 1$ , and the initial conditions  $(x_1, x_2, x_3) = (1.78, -0.85, -1.30)$ . Bottom: the oscillations for  $a = -1.30$ . The frequency stays constant and the amplitude grows according to the  $1/2$  power scaling law as characteristic of the Hopf bifurcation.

### III. COUPLED “SINGLE-DOMAIN” MAGNETIC SYSTEMS

The above preamble leads to a fundamental question: can the emergent oscillatory behavior be observed under different system preparations and constraints? We search for answers using coupled magnetic “fluxgate” magnetometers as an example [1]. We write the system equations for a ring of  $N$  fluxgates, coupled in a directed fashion, in the following form:

$$\begin{aligned}
 \dot{x}_1 &= -x_1 + \tanh[c(x_1 + \lambda x_2 + \varepsilon)], \\
 \dot{x}_2 &= -x_2 + \tanh[c(x_2 + \lambda x_3 + \varepsilon)], \\
 &\vdots \\
 \dot{x}_N &= -x_N + \tanh[c(x_N + \lambda x_1 + \varepsilon)],
 \end{aligned}
 \tag{2}$$

where  $x(t)$  represents the (suitably normalized) magnetic flux at the output (i.e., in the secondary coil) of each unit, and  $\varepsilon \ll U_0$  is an externally applied dc magnetic flux. It is important to note that the oscillatory behavior occurs even for  $\varepsilon = 0$ ; however, when  $\varepsilon \neq 0$ , the oscillation characteristics change. These changes are being exploited for signal quantification purposes; hence we will include the dc signal in the dynamics (2) throughout this work. The elements (i.e., mag-

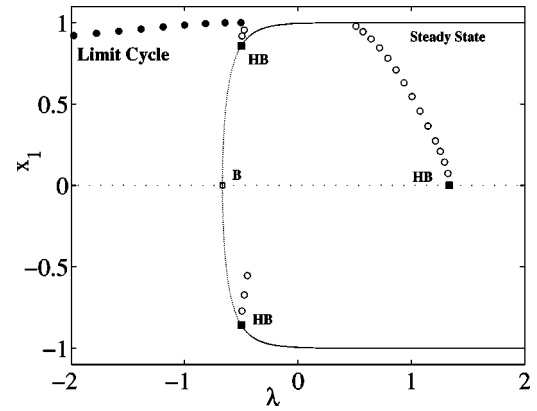


FIG. 2. Bifurcation diagram for a system of  $N=3$  identical fluxgates coupled in a directed ring. Filled-in squares represent local Hopf bifurcations of unstable periodic solutions (empty circles); empty square describes a steady-state pitchfork bifurcation point of two branches of nontrivial unstable equilibria (dotted lines). Filled-in circles represent stable periodic solutions created via global bifurcations.  $c=3, \varepsilon=0$ .

netometers) in (2) are assumed to be identical,  $c$  is a temperature-dependent nonlinearity parameter (each element is bistable for  $c > 1$ ), and  $U_0$  is the energy barrier height of any of the elements, absent the coupling. Notice that the (unidirectional) coupling term, having strength  $\lambda$ , which is assumed to be equal for all three elements, is *inside* the nonlinearity, a direct result of the mean-field nature of the description (in the fluxgate magnetometer, the coupling is through the induction in the primary or “pickup” coil).

#### A. Bifurcation analysis

We begin by enunciating some of the results that have already been presented in [1,3], confining ourselves to the  $N=3$  case (the extension to arbitrary  $N$  will become clear later on), thereby setting up the context of the problem at hand. The bifurcation diagram for this case is given in Fig. 2.

A simple numerical integration of (2) (starting with *non-identical* initial conditions) reveals oscillatory behavior for  $\lambda < \lambda_c$ , where  $\lambda_c$  is a critical (or threshold) value of the coupling strength (as seen in [1],  $\lambda_c < 0$ , so that  $|\lambda| > |\lambda_c|$  in the oscillatory regime). The oscillations are nonsinusoidal, with a frequency that increases as the coupling strength decreases away from  $\lambda_c$ . For  $\lambda > \lambda_c$  (or, equivalently,  $|\lambda| < |\lambda_c|$ ), however, the system quickly settles into one of its steady states, regardless of the initial conditions; the same result ensues if  $N$  is even, or if the coupling is bidirectional. As a side note, we point out that the appearance of oscillations for  $\lambda < \lambda_c$  does not violate any conservation laws; in a practical implementation, some onboard power (e.g., to drive the coupling circuit) is always present. The dc target signal  $\varepsilon$  has the effect of skewing the potential function (for zero coupling) of each element. This has implications for the oscillation frequency as well as the residence times (or, equivalently, the zero crossings) of individual elements of the connected array, in their stable attractors. In previous work [2], we have exploited the induced asymmetry mentioned above in a design

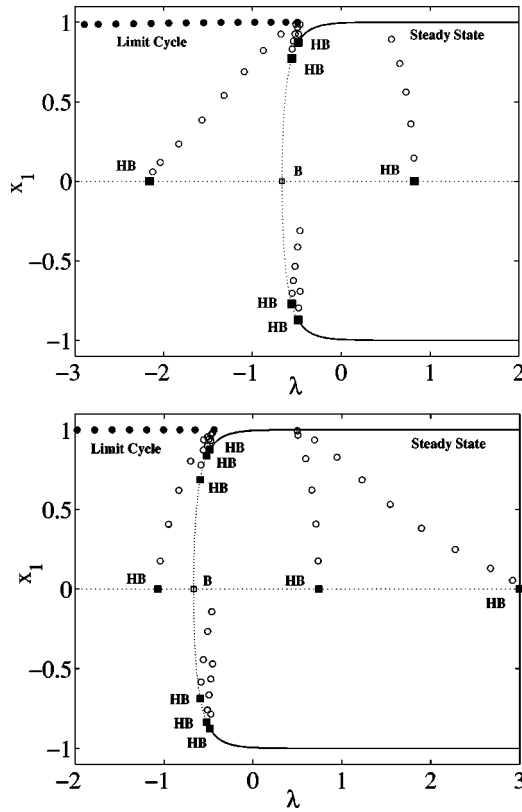


FIG. 3. Bifurcation diagram for a coupled-fluxgate system similar to that used in Fig. 2, except for larger odd values of  $N$ . In both cases, only the branch of periodic solutions that emerges via a heteroclinic orbit (filled-in circles) is stable. (a)  $N=5$  (top) and (b)  $N=7$  (bottom).

for an inexpensive, low-power, and simple to operate fluxgate magnetometer.

For larger odd values of  $N$ , and still unidirectional coupling among nearest neighbors, the system dynamics is more complicated than in the previous case with  $N=3$ . For  $N=5$ , for instance, Fig. 3(a) shows the existence of three additional branches of periodic solutions created via local Hopf bifurcations. One branch is created off the trivial solution  $x_1 = \dots = x_5 = 0$ , while the other two emerge from the nontrivial steady states. All Hopf branches are unstable, so that the only *observable* oscillatory behavior still originates from the heteroclinic cycle—as happens in the  $N=3$  case. This also holds true for larger odd values of  $N$  except that as  $N$  increases the amplitude of the observable oscillations asymptotically approaches unity, and more branches of unstable periodic solutions bifurcate from the nonzero steady state. Figure 3 depicts these facts for two coupled systems with  $N=5$  and  $N=7$  fluxgates. Other cases are similar but are not shown for brevity.

For even values of  $N$ , and preserving unidirectional coupling between nearest neighbors, the system also undergoes a series of Hopf bifurcations, but all of the branches are unstable and, hence, unobservable. Figure 4 shows representative examples for  $N=4$  and  $N=6$ .

While more specialized coupling schemes are beyond the purview of this paper, we have also investigated different

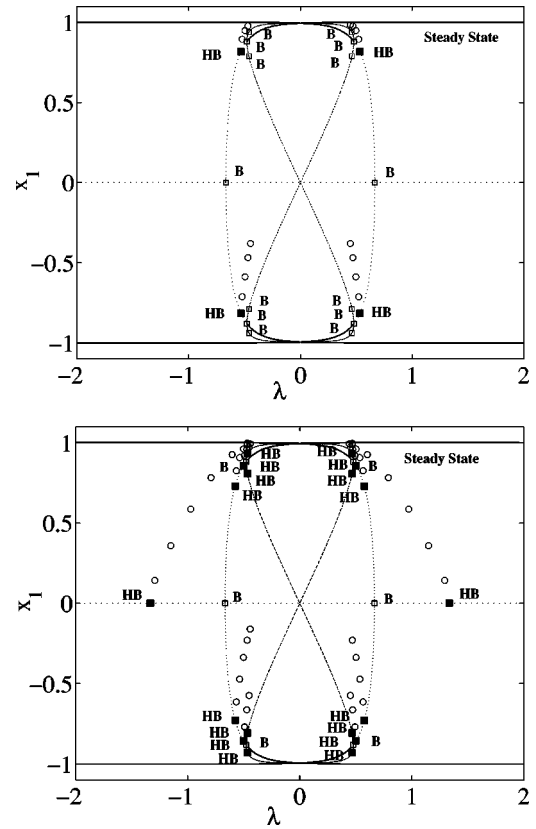


FIG. 4. Bifurcation diagram for a coupled-fluxgate system similar to that used in Fig. 2, except for larger even values of  $N$ . All branches of periodic solutions (empty circles) are unstable. The dotted curves (part of the figure-8 loop) represent the unstable steady state solutions. (a)  $N=4$  (top) and (b)  $N=6$  (bottom).

coupling topologies that include bidirectional coupling among nearest neighbors, unidirectional coupling for nearest neighbors combined with bidirectional coupling between nonnearest neighbors, and unidirectional coupling for nearest neighbors combined with unidirectional coupling between every other nonnearest neighbor. It is worth mentioning that additional coupling facilitates the existence of oscillatory behavior but aside from a potential enhanced tolerance to background noise, with a concomitant enhancement of sensitivity (this will be described in an upcoming paper), increasing the number of elements or rearranging the network to have a different coupling topology does not seem to increase performance as quantified, for example, by the sensitivity of the oscillation frequency to small changes in an applied dc target signal. These issues will be addressed in future work. In summary, from the application point of view, the  $N=3$  case, as presented in [1] and in this paper, is the simplest, and most relevant, case to realize.

### B. Frequency dependence

In [1] we published a numerically derived expression for the oscillation frequency, pending a more detailed theory. We also computed the critical coupling strength  $\lambda_c$  past which the oscillations emerged, via very simple stability arguments. It was further observed that the sum  $X(t) = \sum_i x_i(t)$  could be a

useful quantity for device applications; the period of the summed response was seen to be  $T_i/N$ , where  $T_i$  is the period of individual oscillations in an  $N$ -coupled ring. Finally, we noted that the individual responses  $x_i(t)$ , while having the same frequency [assuming that the parameters  $c$  and  $\lambda$  are the same throughout the dynamics (2)], are offset in phase by  $2\pi/N$ . Increasing  $N$  leads to different frequencies for the individual elements  $x_i(t)$ , with a concomitant phase difference between solutions; however, the summed response has a frequency that is *independent* of  $N$ , as long as the other parameters  $c$  and  $\lambda$  remain unchanged. This will become apparent in what follows. Figure 5 shows the oscillations and the summed response in the system (2), and different values of the coupling strength  $\lambda$  and dc asymmetrizing signal  $\varepsilon$ . We note that analogous phenomena have been observed [3] in the coupled Duffing network (1).

Next we develop a more detailed description of the system dynamics, beginning with a very simple two-state representation that reproduces some of the salient features of the behavior seen in Fig. 5. This is followed by an analysis of the coupled system dynamics, just past the critical point. In particular, we derive an expression for the oscillation period in terms of the separation  $\lambda_c - \lambda$  [recall that  $\lambda, \lambda_c < 0$  in the convention adopted in (2), so that the separation is a positive quantity for  $\lambda < \lambda_c$ ]. We also obtain expressions for the time spent in each of the two stable attractors of the potential energy functions that describe the individual elements in (2) in the absence of coupling; in turn, this leads us to an expression for the residence time difference (RTD), a quantity that directly reflects the asymmetrizing signal  $\varepsilon$ ; for  $\varepsilon=0$ , the potential functions are symmetric, and the (deterministic) residence times the same.

#### IV. A SIMPLE (TWO-STATE) DESCRIPTION OF THE DYNAMICS

Just past the critical point, it is evident from Fig. 5 that each state point spends the bulk of its time trapped in one of the stable attractors at  $\approx \pm 1$ , with a negligible amount of time lost in the ‘‘hop’’ to the opposite attractor (potential minimum). The exact locations of these attractors can be computed via the single-element dynamics, as was done in [2] for the bistable case  $c > 1$ . Accordingly, one needs to compute only the time required for a given element to evolve from one of its stable attractors to the corresponding inflection point; these points are located (for  $\lambda = 0$ ) at  $\pm x_{inf} = \pm \sqrt{(c-1)/c}$  (see [2] for more details). Note that the fixed points (observed from the time-dependent solutions) of each potential remain at approximately  $\pm 1$  even for finite  $\lambda$ ; however, they cannot be as readily calculated via a potential function as in the uncoupled system.

In this section, we will simplify the original model to various degrees. Our goal is to examine a model that can be treated analytically but is still able to capture the essential features of the original model. We will first study the most drastic simplification possible, in which we replace the nonlinear hyperbolic tangent by the sign function. This model can be solved exactly and can shed light on some of the striking dynamics we have described above. In particular, it

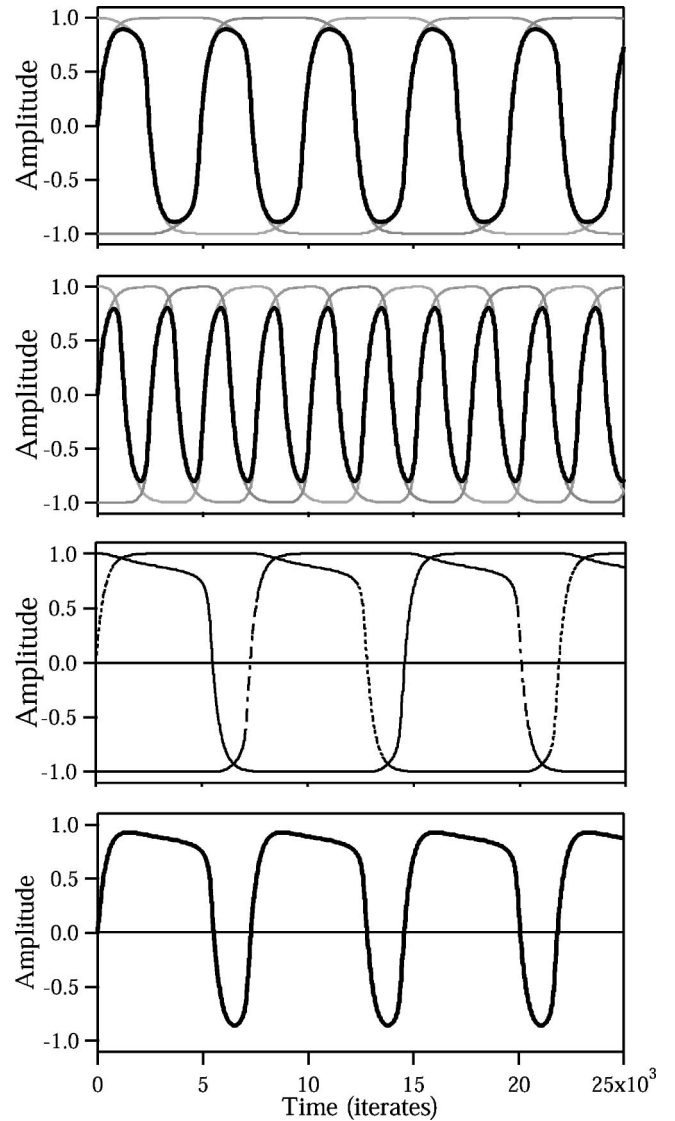


FIG. 5. Emergent oscillatory behavior in the coupled system (2) for  $N=3$ . The top panel shows the oscillations near the critical point. Summed response is indicated by thick black lines, and individual element responses follow the gray lines in all panels. Typical of the heteroclinic cycles, the amplitudes are fully grown at the start of the bifurcation and the frequency is low. At the creation of the oscillations, the frequency is zero as predicated by the heteroclinic bifurcation. The parameters are set at  $\lambda = -0.60$ ,  $\varepsilon = 0$ . The second panel shows the oscillations for a higher coupling strength  $\lambda = -0.75$  and  $\varepsilon = 0$ . Contrasted with the top panel, the frequency scales as a square root of  $|\lambda|$  and  $\varepsilon$ . The third panel shows the individual element oscillations for  $\lambda = -0.60$ ,  $\varepsilon = 0.05$ . Notice that the sum signal (last panel), obtained from the individual oscillations in the third panel, is greatly offset between the upper state (above zero) and the lower state (below zero). Also notice the decrease in frequency when the target signal  $\varepsilon$  is nonzero compared to the top panel. The initial conditions for all simulation runs are  $(x_1, x_2, x_3) = (1.0, 0.0, -1.0)$ ,  $c = 3$ , and the time step size is 0.002 68. For each panel, the critical coupling  $\lambda_c$ , at the onset of the oscillations, may be determined from Eq. (5) of [1] or, equivalently, from Eq. (18) below.

offers insight into the fact that only a system containing an odd number of elements leads to a time-varying, periodic solution while a system with an even number of elements always relaxes to a steady-state solution. We will then investigate a slightly more complicated model in which we introduce a parameter and for which we can derive a bifurcation threshold and scaling.

**A. A very simple model**

Let us replace the hyperbolic tangent term by its asymptotic values  $\pm 1$ . We are then left with a very simple model:

$$\dot{x}_i = -x_i + \text{sgn}(x_{i+1}). \tag{3}$$

The  $N$  elements are considered to be placed in a ring and  $\text{sgn}(x_{i+1})$  has the usual meaning i.e.,  $\text{sgn}(x_{i+1}) = -1$  for  $x_{i+1} < 0$  and  $\text{sgn}(x_{i+1}) = 1$  for  $x_{i+1} \geq 0$ . Of course, this block-type function is a gross oversimplification of the actual interaction and is, strictly speaking, valid only in the limit of large  $\lambda < 0$ . Nevertheless, the advantage of the above equations is that they are amenable to analytical treatment. The equations have two fixed points  $x = \pm 1$ , and we can obtain the following explicit solution:

$$x_i(t) = \begin{cases} 1 - e^{-(t+k_0)} & \text{for } x_{i+1} < 0, \\ -1 + e^{-(t+k_1)} & \text{for } x_{i+1} \geq 0, \end{cases} \tag{4}$$

where  $k_0$  and  $k_1$  are determined by the initial conditions.

A nonoscillating solution consists of elements in one of the two fixed points. It is easy to show that if element  $i$  is in  $+1$  (i.e., the response amplitude is  $+1$ ), then it is stable only if element  $i+1$  is in  $-1$ . For  $N$  even, a solution consisting of elements alternating in  $+1$  and  $-1$  can thus be found. For  $N$  odd, however, this alternate arrangement is not stable: point  $i=N$  is coupled to  $i=1$  which is in the same fixed point. Thus, this point becomes unstable and switches to the other fixed point. However, since this element is coupled to its preceding neighbor (in this case,  $i=N-1$ ), it will drive the preceding element out of its fixed point. This process repeats itself throughout the ring and a time-dependent solution develops, which is characterized by a soliton-like wave that propagates through the ring. This can be clearly seen in Fig. 6, where we illustrate in a space-time plot the departure from the fixed point, defined here as  $1 - |x_i|$ . The ring in Fig. 6 consists of 55 elements and the ‘‘disturbance,’’ i.e., the location where an element becomes unstable, travels backward through the ring. The initial conditions were set up such that only one such disturbance was created. However, by choosing different initial conditions, it is possible to have more disturbances in the ring.

The period  $T$  of the ensuing oscillation can be found analytically for large  $N$ . This is aided by the fact that for these values of  $N$  the period becomes large enough for an individual element to reach one of the fixed points. The element will remain in this fixed point until its forward neighbor changes sign. This can be seen in Fig. 7, where we have plotted the time trace of one of the elements in the ring of

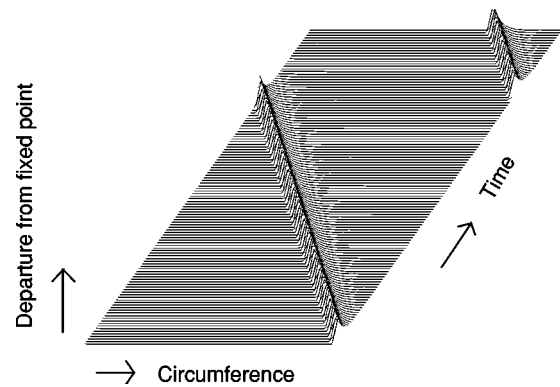


FIG. 6. Space-time plot of the departure from the fixed point (defined here as  $1 - |x_i|$ ) for a ring of  $N=55$  elements (see text for explanation).

Fig. 6, along with its forward neighbor. For this case, a time trace of an individual element can be accurately described, after a suitable shift in time, by

$$x(t) = \begin{cases} -1 + 2e^{-t} & \text{for } 0 \leq t < \frac{T}{2N}, \\ 1 - 2e^{-(t-T/2N)} & \text{for } \frac{T}{2N} \leq t < \frac{T}{N}. \end{cases} \tag{5}$$

This element will cause its neighbor to become unstable when it crosses zero. The time needed for this,  $t^*$ , can be easily calculated:

$$0 = -1 + 2e^{-t^*}, \tag{6}$$

and we find  $t^* = \ln(2)$ . Thus, the period is given by  $T = 2N \ln(2)$ . In practice, we find that this approximation already works well for  $N$  as small as 9. This can be seen in Fig. 8, where we have plotted  $T$  as a function of  $N$  found in the simulations of the full system (open circles) and as predicted by the above expression (solid line).

Finally, let us address the dynamics of the average of the elements. The equation for this average  $X = (1/N) \sum x_i$ ,

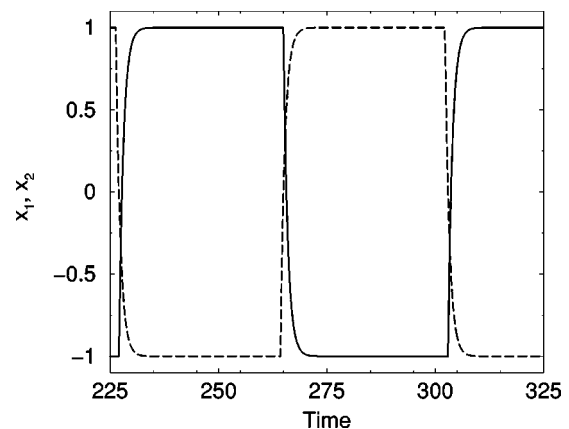


FIG. 7. Response of a single element (solid line) and its forward neighbor (dashed line), which are part of a  $N=55$  ring, vs time (seconds).

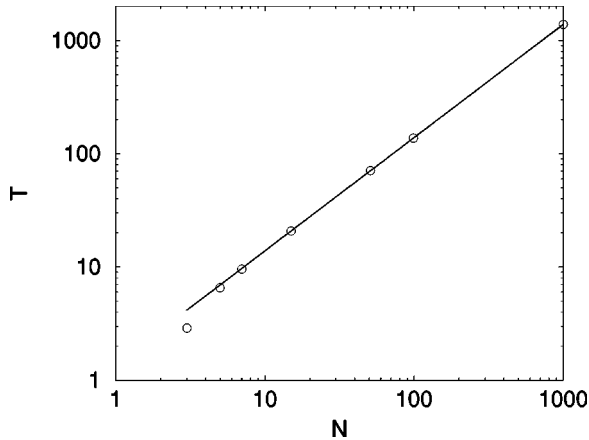


FIG. 8. The period (seconds) as a function of the number of elements for the very simple model (circles) and for the analytical approximation (solid line).

$$\dot{X} = -X - \sum \text{sgn}(x_{i+1}), \quad (7)$$

shows that  $X=0$  is a solution. For  $N$  even, this can be easily attained by choosing the alternating sign solution. For  $N$  odd, as discussed above, this solution is unstable and a time-periodic solution develops. Interestingly, the period of the average  $X$ ,  $T_X$ , is independent of the number of elements and reads  $T_X = 2 \ln(2)$ .

### B. A slightly less simple model

Clearly, the system analyzed above is an oversimplification of the full system since, even though it can capture some of the salient features, it does not undergo a bifurcation as a parameter is varied. To introduce a bifurcation parameter, we extend the simple model of the preceding subsection to include interelement coupling:

$$\dot{x}_i = \begin{cases} -x_i + \text{sgn}(\lambda) \text{sgn}(x_i) & \text{for } |\lambda x_{i+1}| < \alpha, \\ -x_i + \text{sgn}(\lambda x_{i+1}) & \text{for } |\lambda x_{i+1}| \geq \alpha, \end{cases} \quad (8)$$

where we have introduced  $\alpha$  as a new parameter. Note that this is, in some sense, equivalent to replacing the hyperbolic tangent by the dominant pieces of its argument. As before, we get a soliton-like wave propagating through the ring and, for large  $N$ , we can again approximate the exact solution by

$$x(t) = -1 + 2e^{-t}, \quad (9)$$

where we have shifted time and written down only the “downward” part of the solution. As the element leaves its fixed point, the preceding element will become unstable. In the oversimplified model of the preceding subsection, the condition for this event was that the element cross 0. Now, however, the condition becomes

$$\frac{\alpha}{\lambda} = -1 + 2e^{-t^*}. \quad (10)$$

Thus, we find  $t^* = -\ln(1/2 - \alpha/2\lambda)$  and the (single-element) period is given by  $T = 2N \ln(2\lambda) - 2N \ln(\lambda - \alpha)$ . The expression for  $t^*$  also gives us immediately the critical  $\lambda, \lambda_c$ :

$$\lambda_c = \alpha. \quad (11)$$

The period diverges as  $\lambda \rightarrow \lambda_c$ ; this has already been observed in our earlier work [1] wherein we carried out a simulation of the coupled system (2).

### V. DYNAMIC DESCRIPTION NEAR THE CRITICAL POINT

We now turn to a more detailed description of the dynamics of (2), confining ourselves to the immediate neighborhood of the critical point in the oscillatory regime, i.e., when the separation  $\lambda_c - \lambda$  is small. We note, however, that our results provide a very good description of the dynamics (in particular, the scaling of the oscillation period with the coupling strength and/or symmetry-breaking signal) well past the onset of the oscillations. This will become apparent later in this section. We carry out the analysis for  $N=3$  elements; the generalization to arbitrary  $N$  will be made clear at the end. We refer to Fig. 5, specifically the third and fourth panels which correspond to the case of small separation  $\lambda_c - \lambda$ . Note that Fig. 5 was generated using a specific set of initial conditions; however, the analysis will make clear that the dynamics evolve independently of this choice, as long as at least one element has an initial state different from the others.

Many of the observations of the preceding sections are immediately apparent from Fig. 5. For small separation  $\lambda_c - \lambda$ , it is clear that the state points spend the bulk of their transition times reaching the inflection points  $\pm x_{inf} = \pm \sqrt{(c-1)/c}$ , after which the passage to the opposite minimum (at  $\pm 1$ ) is very rapid (this is particularly obvious in Fig. 7). Put differently, the combination of dc and coupled fluxes in each of the elements of (2) causes that particular potential to skew or tilt so that a minimum and the saddle point approach each other, coalescing into an inflection point. At this point, an infinitesimal further tilt causes the state point to drop into the opposite minimum, all the time providing an input to the next (forward-coupled) element via the coupling, so that a solitonlike periodic disturbance travels around the ring. One also notes that the elements evolve two at a time, with one element always remaining in its steady state while the others evolve. This behavior, which is most pronounced near the critical point, has already been observed in the simplified descriptions of the preceding section (see, e.g., Fig. 7), and is reminiscent of what might be expected in a discrete line of magnetic spins, subject to a dc magnetic field. For an odd number of spins, there will always be two spins that have the same alignment and are therefore “frustrated,” with each spin trying to orient itself antiparallel to the other.

It is also clear (Fig. 5) that the zero-crossing points  $t_0 (=0)$ ,  $t_1$ ,  $t_2$ , etc., of the summed output  $X(t)$  also correspond to the crossing points of the individual elements, e.g.,  $t_1$  corresponds to the zero crossing of  $x_1(t)$ ,  $t_2$  for  $x_3(t)$ , etc. Hence, the problem of finding the period  $T_+$  of the summed output, or the individual oscillation periods  $T_i \equiv T_3$  (which are all the same; the suffix refers to the  $N=3$  case) reduces to determining the zero-crossing times  $t_{1,2}(t)$ .

From our discussion above it is evident that, during the dominant part of the evolution of  $x_1(t)$  (in Fig. 5 this corre-

sponds to the half-cycle starting at  $x_1=1$ ), the element  $x_2(t)$  remains in its steady state  $x_+ \approx 1$  (the exact locations of the fixed points can be readily found via simple calculus, as was done in [2], and for  $c > 1$  are very close to  $\pm 1$ , due to the tanh function) so that the first of the equations (2) can be simplified to

$$\dot{x}_1(t) = -x_1 + \tanh c(x_1 + \lambda + \varepsilon), \quad (12)$$

corresponding to simple ‘‘particle-in-potential’’ motion. Formally integrating this equation yields

$$t_1 = \int_1^0 \frac{dx_1}{\tanh c(x_1 + \lambda + \varepsilon) - x_1}, \quad (13)$$

where  $t_1$  is the time taken (for this choice of initial conditions) by the state point  $x_1(t)$  to evolve from its attractor at +1 to 0 (Fig. 5). This integral cannot be evaluated analytically, in general. Similarly, we see that  $x_3(t)$  evolves while  $x_1(t) \approx -1$  so that we have

$$\dot{x}_3(t) = -x_3 + \tanh c(x_3 - \lambda + \varepsilon), \quad (14)$$

whence we obtain

$$t_{12} \equiv t_2 - t_1 = \int_{-1}^0 \frac{dx_3}{\tanh c(x_3 - \lambda + \varepsilon) - x_3}. \quad (15)$$

From these two integrals, we may write down the period  $T_+$  of the summed output as  $T_+ = t_{12} + t_1$  by formally summing the above expressions. A little manipulation of the integration limits shows immediately that  $T_+ = 2t_1$  for  $\varepsilon = 0$ , as expected. Having obtained the above expressions, it is easy to see that  $t_3 = T_+ + t_1, t_4 = 2T_+, t_5 = 2T_+ + t_1, t_6 = 3T_+$ , etc. In particular, we can write down the expression for the individual periods as  $T_3 = 3T_+$ , and for the phase differences between individual solutions as  $t_3 - t_1 = t_5 - t_3$ , etc., so that the phase difference is  $2\pi/3$ .

The generalization of the above observations to arbitrary  $N$  should now be clear. In this case, the individual periods (and the phase offsets) do change; however, again, only two elements are simultaneously evolving at any given time, the remainder staying in their steady states. Hence, the period of the summed output is always the same, and we obtain,  $T_+ = T_i/N$  where  $T_+$  is now the summed output of  $N$  (odd) elements, and  $T_i$  is the period of the individual oscillations for the  $i=N$  case. The phase offset between solutions for arbitrary  $N$  is  $2\pi/N$ . It is worth noting that increasing  $N$  leads to a concomitant increase in the period of the individual oscillations. A similar result was obtained by us [7] in a different system, a globally coupled network of dc superconducting quantum interference devices whose individual elements could undergo saddle-node bifurcations to oscillatory behavior in the absence of the coupling.

Referring now to the summed output  $X(t)$ , the difference in zero-crossing times is a direct marker of the asymmetrizing target signal  $\varepsilon$ . We write this as  $\Delta t = t_1 - t_{12}$  which, after some manipulations, can be written as

$$\Delta t = \int_0^1 dx \left[ \frac{1}{\tanh c(x + \lambda - \varepsilon) - x} - \frac{1}{\tanh c(x + \lambda + \varepsilon) - x} \right], \quad (16)$$

which for small  $\varepsilon$  may be written as,

$$\Delta t \approx 2c \varepsilon \int_0^1 dx \frac{\text{sech}^2 c(x + \lambda)}{[\tanh c(x + \lambda) - x]^2}. \quad (17)$$

This result shows that  $\Delta t$  is proportional to  $\varepsilon$  for small (compared to the energy barrier height) target signals, a result that has already been quantified [2] in single-fluxgate magnetometer experiments. In this regime, we may define a sensitivity  $S$  via the derivative  $\partial \Delta t / \partial \varepsilon$ , yielding an expression that is independent of  $\varepsilon$ . For a practical system, this is a desirable result. It is also obvious that the RTD and the associated sensitivity would be the same if we chose to compute them via the zero crossings of any one of the solutions  $x_i(t)$ , rather than the sum. Note, also, that the oscillations shown in Fig. 5 are *suprathreshold*, an important point, since it mitigates the effect of noise and allows a ‘‘natural’’ operation with an effectively suprathreshold bias signal; by contrast, we point to the  $N=1$  case [2] wherein the oscillations were generated onboard the (single) device through an external source with controllable amplitude and frequency. Note that, theoretically at least, the optimal operating point for a single bistable device corresponds to a bias signal that is slightly *subthreshold* [8]. In this regime, a combination of the signal and background noise induces hopping between the stable steady states of the potential. However, practical issues, e.g., the longer observation times required in the presence of a nonnegligible noise background, often preclude operation in this regime.

It is easy to plot the quantities expressed via the formal integrals (13) and (15). Before doing so, however, we derive analytic expressions for the period  $T_+$  when the separation  $\lambda_c - \lambda$  is very small. We note that the procedure of this section starts to break down when  $|\lambda|$  increases significantly past  $|\lambda_c|$ , because the approximation of assuming that the elements evolve only two at a time with the rest of them remaining fixed at their (constant) steady-state values throughout the evolution becomes increasingly tenuous, and we can no longer replace the coupling factors (inside the nonlinearities) by constants. This is evident from the right panels of Fig. 5. For this situation, one must compute the period via direct integration of the original coupled system (5), although qualitative behavior can still be very well predicted using the approximate theory.

The integrals in Eqs. (13) and (15) may be evaluated just past the critical point, where the integrands display sharply peaked behavior. We start with (13) and note that the denominator is sharply peaked at  $x = x_m$ , a value that can be found by differentiation as  $x_m = -\lambda - \varepsilon + (1/c) \tanh^{-1} x_{inf}$  where  $x_{inf} = \sqrt{(c-1)/c}$  denotes the location of the point of inflection. The critical coupling at which the potential function corresponding to the  $x_1$  dynamics has an inflection point may be obtained by setting  $f(x_{inf}, \lambda_c) = 0$ ,  $f(x, \lambda)$  being the denominator in the integrand of (13). We readily obtain



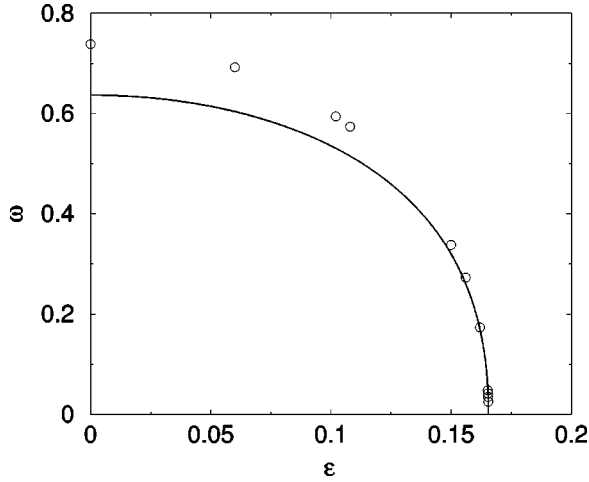


FIG. 9. The angular frequency of the summed response calculated via direct numerical simulations (solid line) and via the approximate relationship in Eq. (22) vs dc target signal amplitude  $\varepsilon$ . Parameter values are  $N=3$ ,  $c=3$ , and  $\lambda=-0.6$ , giving  $\varepsilon_c \sim 0.1656$ .

$$\lambda_c = -\varepsilon - x_{inf} + \frac{1}{c} \tanh^{-1} x_{inf}, \quad (18)$$

so that  $x_m = \lambda_c - \lambda + x_{inf}$ . We now expand the denominator  $f(x)$  about  $x = x_m$  obtaining, after some algebra,

$$f(x) \equiv \tanh c(x + \lambda + \varepsilon) - x \approx \lambda - \lambda_c - cx_{inf}(x - x_m)^2. \quad (19)$$

Then, finally, we can evaluate the integral in (13), extending the limits to  $\pm\infty$  (because of the sharply peaked nature of the integrand):

$$t_1 \approx \int_{-\infty}^{\infty} \frac{dx}{\lambda_c - \lambda + cx_{inf}(x - x_m)^2} = \frac{\pi}{\sqrt{cx_{inf}}\sqrt{\lambda_c - \lambda}}. \quad (20)$$

In an analogous way, we can develop a closed form expression for the integral in (15):

$$t_{12} \approx \int_{-\infty}^{\infty} \frac{dx}{\lambda_c - \lambda + 2\varepsilon + cx_{inf}(x - x_{mm})^2} = \frac{\pi}{\sqrt{cx_{inf}}\sqrt{\lambda_c - \lambda + 2\varepsilon}}, \quad (21)$$

where  $x_{mm} = \lambda - \varepsilon - (1/c)\tanh^{-1} x_{inf} = -x_m$ . The oscillation period  $T_+$  of the summed response is then obtained by summing the last two expressions to yield

$$T_+ = \frac{\pi}{\sqrt{cx_{inf}}} \left[ \frac{1}{\sqrt{\lambda_c - \lambda}} + \frac{1}{\sqrt{\lambda_c - \lambda + 2\varepsilon}} \right]. \quad (22)$$

A comparison between the result obtained from this expression and from direct numerical simulations is presented in Figs. 9 and 10. This comparison shows that the analytical expression captures the dynamics well, especially near the bifurcation threshold, but also well into the oscillating regime. This is attributable to the fact that the peaked nature of the denominators of Eqs. (13) and (15) persists well into the oscillating regime, even though the peaks get broader as one moves deeper into this regime.

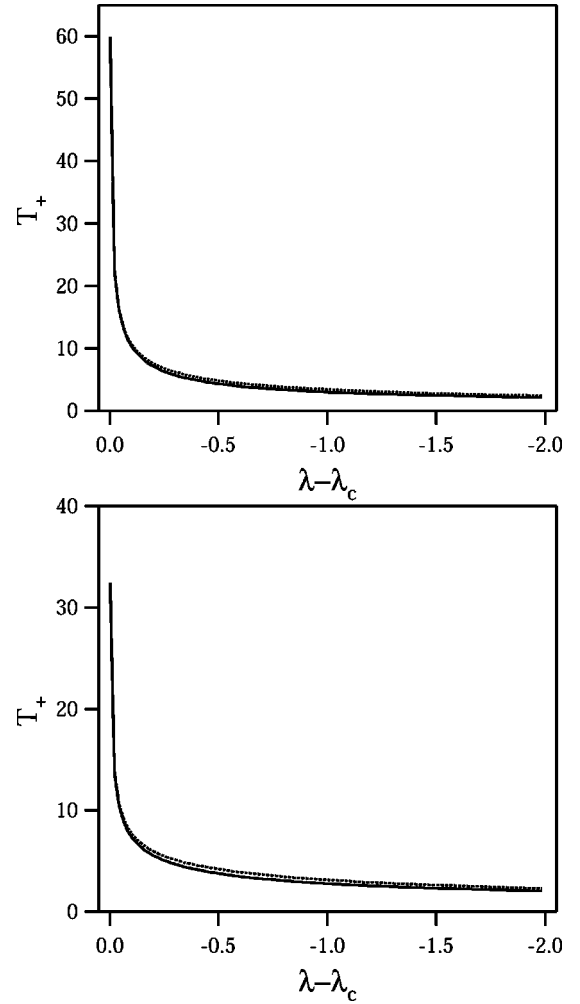


FIG. 10. Period  $T_+$  (seconds) of the summed signal obtained via numerical simulation of the dynamics (2) (solid curve) and via the expression (22) (dotted curve) vs bifurcation "separation"  $\lambda - \lambda_c$ . Top:  $c=4, \varepsilon=0$ . Bottom:  $\varepsilon=0.2$ . The approximation agrees very well with the numerically obtained period, even for large  $\lambda$  and  $\varepsilon$ .

In the immediate vicinity of the critical point, i.e.,  $\lambda_c - \lambda$  is positive and small, we may approximate the period of the summed oscillation by Eq. (22), which displays the inverse square-root scaling behavior that one should expect. Note that  $\lambda_c = \lambda_c(\varepsilon)$  which leads to  $T_+ = 2t_1$  in the absence of the asymmetrizing signal  $\varepsilon$ . This behavior is captured in Fig. 10 where we plot the period of the summed signal obtained by direct integration of the dynamics (2), vs the approximation (22). It is seen that (22) provides a good answer everywhere, especially for very small separations  $\lambda_c - \lambda$ . It is worth noting that we can carry out a small- $\varepsilon$  expansion for the period:

$$T_+ \approx \frac{\pi}{cx_{inf}\sqrt{\lambda_{c0} - \lambda}} \left[ 2 + \frac{3}{4} \left( \frac{\varepsilon}{\lambda_{c0} - \lambda} \right)^2 + O(\varepsilon^4) \right] = T_{+0} + \text{const} \times \varepsilon^2, \quad (23)$$

which is valid for  $\varepsilon \ll \lambda_c - \lambda$ , with  $\lambda_{c0} = -x_{inf} + (1/c)\tanh^{-1} x_{inf}$  the critical coupling for the onset of oscillations in the absence of the asymmetrizing signal.

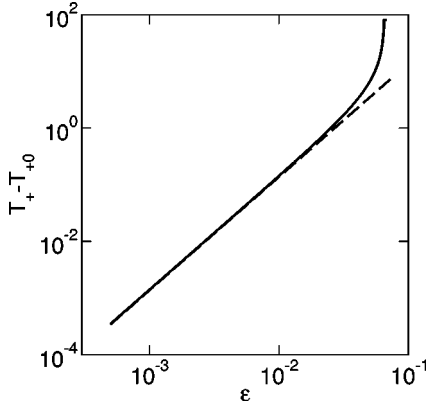


FIG. 11. The period  $T_+$  of the summed oscillation, reduced by the period for  $\epsilon=0$ , as a function of  $\epsilon$ . The results from the Taylor expansion (23) are plotted as a dashed line while the results from the direct numerical calculation are plotted as a solid line. The curve obtained via the expression (22) is indistinguishable from the solid curve at this scale.  $N=3$ ,  $c=3$ ,  $\lambda=-0.5$ .

The approximations to the times  $t_1$  and  $t_{12}$  lead, directly, to an approximate expression for the RTD  $\Delta t(=t_1-t_2)$  close to the critical point:

$$\Delta t \approx \frac{\pi}{\sqrt{cx_{inf}}} \left[ \frac{1}{\sqrt{\lambda_c - \lambda}} - \frac{1}{\sqrt{\lambda_c - \lambda + 2\epsilon}} \right], \quad (24)$$

which also exhibits the square root behavior. Using the last expression, we can obtain an  $O(\epsilon)$  approximation to the RTD:

$$\Delta t \approx \frac{\pi\epsilon}{\sqrt{cx_{inf}}} (\lambda_{c0} - \lambda)^{-3/2}, \quad (25)$$

so that the sensitivity  $\partial\Delta t/\partial\epsilon$  is enhanced as we get closer to the critical point, where we note that decreasing the temperature-dependent control parameter  $c$  close to unity, can also lead to enhanced sensitivity to small  $\epsilon$ , as is readily apparent in (25). It is worth pointing out that a sensitivity  $\partial T_+/\partial\epsilon$ , defined via the oscillation period, is actually a function of  $\epsilon$ . This may not be desirable in practical sensors where one would like to develop the optimal sensor configuration independently of the target signal. From this standpoint, the RTD may constitute the more reliable measure. Note also that, when  $\epsilon$  becomes comparable to the separation  $\lambda_c - \lambda$ , the expansions (23) and (25) do not agree well with simulations. This is apparent in Fig. 11, where we have plotted  $T_+ - T_{+0}$  using direct numerical simulations and the expansion (23) as a function of  $\epsilon$ .

**VI. EXPERIMENTS**

We now turn to a description (Fig. 12) of the experiments carried out on a three-fluxgate setup. The printed circuit board (PCB) technology based fluxgates [9] have cores made of cobalt-based Metglas 2714A material, and each is sandwiched between two sheets of PCB material. The sides of the PCB sheets that face away from the core material are printed with copper wirings to form the windings of the driving coil

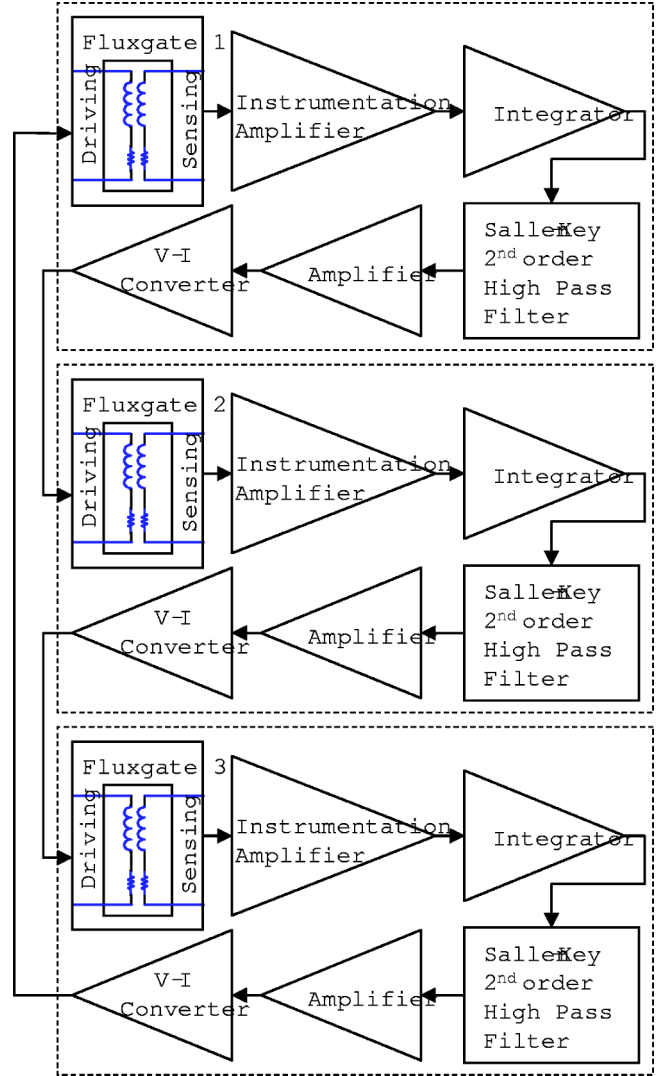


FIG. 12. Flow diagram for the coupled-fluxgate experiment. Each fluxgate consists of two coils, the sensing coil and the driving coil. Starting with fluxgate 1, the signal from the sensing coil first goes through the current-to-voltage converter. Then it passes through the “leaky” integrator, followed by a Sallen second-order filter before going through the main gain stage. Thereafter, the signal goes through the voltage-to-current converter and then it connects to the drive coil of the adjacent fluxgate (fluxgate 2). The other two fluxgates are connected in the same manner.

and the sensing coil. Solder is used to fuse the two sheets together to complete the circuit for the windings. The fluxgates are then coupled through electronic circuits where the (voltage) readout of one fluxgate signal (i.e., the derivative signal of the flux detected by the sensing coil) is amplified by a voltage amplifier with a very high impedance, which also trims out any dc in the output. Following this, the signal is passed through a “leaky” integrator to convert the derivative signal seen by the sensing coil back to the “flux” form so that the experimental system closely conforms to the model (2). The use of a “leaky” integrator at this stage also helps to avoid the divergence caused by a small dc signal that might have leaked through the voltage amplifier stage. Typically the integrator output contains a dc component that must be

removed before the signal is passed to the other fluxgates. This is accomplished by employing a Sallen-Key second-order high-pass filter immediately after the integrator, with the parameters tuned to work at a specific frequency (the mean oscillating frequency of the coupled system). The signal then passes through an amplifier to achieve adequate gain to drive the adjacent fluxgate. After this, the signal passes through a voltage-to-current converter ( $V-I$  converter) in its final step to drive the primary coil of the adjacent fluxgate. This converter also has a gain factor but it is fixed to a certain value during the construction of the coupling circuits. The gain is set at much less than unity so that one volt in the signal does not convert to one ampere in the voltage-to-current converter stage. The setup repeats for the other two coupling connections for the remaining fluxgates and all values of the coupling circuit parameters are closely matched from one set to the other. Each stage of the coupling circuit also employs high speed and high precision operational amplifiers to minimize the time delay in order to conform closely to the model since knowledge of state variable  $x_i$  is known instantly in the model.

The oscillations observed from this setup are quite striking (Fig. 13). The system readily oscillates in a traveling pattern. Like the model, the system favors this pattern no matter how many times it is restarted. The frequency of oscillations is about 57 Hz. Each wave is phase shifted by exactly  $2\pi/3$  as predicted by the model. Comparison of the oscillations from the experiment to the numerical results shows good agreement. Both wave forms are qualitatively similar, but the wave form from the experiment is a mirror image of the wave form from the model. This is probably due to the inversion of the winding of the coils in the construction of the fluxgates. In addition, since we do not know the value of  $c$  and the time constant  $\tau$  in the actual device (we set  $\tau=1$  in the model), we cannot correctly compare the time scales in the model and the experimental observations. The amplitudes of the oscillations in the experiment are also arbitrary compared to the model because the recorded voltages depend on the gains set in the coupling circuit. On the other hand, the magnetic flux in the model saturates between  $\pm 1$ , but in the fluxgate devices this quantity cannot be measured directly.

## VII. CONCLUSION

We have illustrated the idea that overdamped systems can be made to produce self-sustained oscillations when the coupling topology is judiciously chosen. Even though our treatment is largely limited to the unidirectionally coupled system on a ring, the idea can be extended to other coupling topologies that can be bidirectional or a combination of unidirectional and bidirectional coupling; as briefly discussed in Sec. III, these alternate coupling topologies can also lead to the emergence of oscillations. Of course there are endless coupling configurations that one can pursue and explore, but there is something special for the case of a unidirectional coupling case being discussed here. With a unidirectionally coupled case, the oscillations stem from a heteroclinic cycle bifurcation. There are Hopf bifurcations occurring off of the

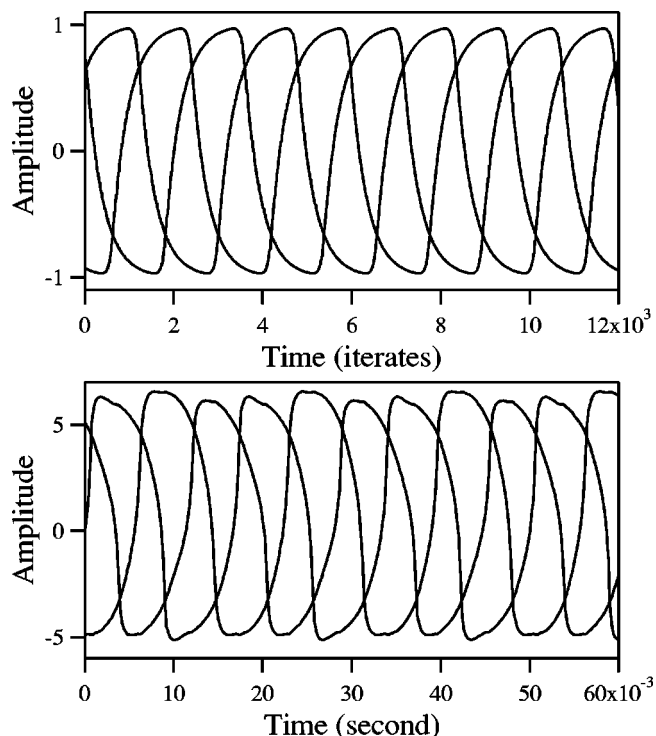


FIG. 13. Top: the numerical data for  $c=4$ ,  $\lambda=-1.55$ , and  $\epsilon=0$ . Curves represent the solutions  $x_i(t)$ ,  $i=1, 2, 3$ , of the coupled system (2). Bottom: the experimental data from three coupled PCB fluxgate magnetometers. There is very good qualitative agreement between the model and the experimental systems as indicated by the similarity of the wave forms between top and bottom panels. The experimental system lacks a couple of parameters (the device time constant  $\tau$  and the  $c$  value) that are necessary for determining the exact frequency to match with the numerical result. The amplitudes of the experimental time series are also on a different scale because the voltages recorded at the output of the experiment are determined by the overall gains in the circuits used to couple the magnetometers.

trivial fixed point  $(0,0,0)$  but none of them is stable. So it is left to the heteroclinic bifurcation to create and annihilate the oscillations with respect to the system parameter. Since there is only one bifurcation responsible for the oscillations, the basin of attraction of this solution is very big. In fact it encompasses almost the entire phase space of the system with the sole exception of a symmetrical space formed by  $x_{i,0} = x_{i+1,0} = x_{i+2,0} = \dots = x_{N,0}$  (the subscript 0 denotes the initial state). Anything deviating from this space, will be attracted toward the oscillatory solution. This is very important from the device stand point because not having to choose the correct initial conditions for a desired solution simplifies the implementation, since setting initial conditions is very difficult to do in practice. From the application point of view, the unidirectional coupling is also simpler to implement electronically. In contrast, for the bidirectional coupling for instance, there are many oscillatory solutions that originate from Hopf bifurcations. Each competes for its basin of attraction. To get to the desired solution, one must choose the correct initial conditions which is very difficult to do in practice.

The derived analytical expression for the oscillation periods agrees with the numerical results from the simulation of the full system dynamics. Since we are using the residence-times-based method to detect the asymmetry-inducing external dc field, knowing the oscillation period aids in determining the operational location of the device with respect to the bifurcation point. It is worth pointing out that the oscillations in the coupled system are always suprathreshold (in each of the potential wells corresponding to the individual, uncoupled, devices). This is important, because it enhances the device's tolerance to background noise in real applications. For single-fluxgate magnetometers operated as level crossing detectors, for example, one must prebias the device with a known time-harmonic signal that is taken to be somewhat suprathreshold. As one lowers the amplitude of this signal, noise effects become more important with the residence time distributions developing tails [2]. In this case, the crossing events cannot be clearly noted and longer observation times are necessary to get good crossing statistics. Hence, a device in which the oscillations can be spontaneously generated and are *a priori* suprathreshold, is certainly advantageous; although quantifying the coupling and the separation  $\lambda_c - \lambda$  may be difficult in practice. In a forthcoming paper, we address some of these issues in the framework of a detailed presentation of our experimental results.

We close with a brief overview of ongoing work. Throughout this paper, the target signal  $\varepsilon$  has been taken to be dc and subthreshold, i.e., its amplitude is much smaller than the deterministic switching threshold for an isolated magnetometer; the switching threshold is the value of  $\varepsilon$  that skews the potential energy function just enough to create a point of inflection, so that a minuscule increase in  $\varepsilon$  past this point leads to switching to the opposite magnetization state of the core. One may reasonably ask about the coupled system response to a time-periodic target signal. Calculations and experiments using a time-sinusoidal target signal of fre-

quency  $\omega_t$  have been carried out with striking results: (1) For a coupled system that is already oscillating (through a suitable adjustment of the coupling coefficients) at frequency  $\omega$ , the inclusion of the subthreshold periodic target signal results in the appearance of all the "combination tones"; this is a well-documented effect of mixing two or more frequencies in nonlinear devices (see, e.g., [10] and references therein) at frequencies  $m\omega \pm n\omega_t$ , where  $m, n$  are positive integers that satisfy certain selection rules (depending on the system symmetry). The residence times statistics are no longer a simple marker of the target signal and spectral techniques are necessary. The power spectral density of the response shows the mixing of frequencies very clearly, and one can determine the target signal amplitude and frequency through an analysis of the spectral amplitudes at various frequencies; this has been verified theoretically and also via the experimental setup of Fig. 12. (2) for the case of the system set just prior to the onset of oscillations (in the absence of any target signals), a dc target signal does not elicit oscillatory behavior; this should be apparent from the analysis of this paper. However, a subthreshold time-periodic target signal can induce oscillatory behavior in this setup, if its amplitude and frequency obey certain restrictions. One finds that the *summed* output oscillates at the target signal frequency  $\omega_t$ ; in this case, one can use the residence times technique to quantify the response, since there is only the one frequency  $\omega_t$  present in the output (recall that the system is set up so that there are no oscillations prior to the insertion of the target signal). A subsequent publication will present theoretical and experimental details of this behavior.

#### ACKNOWLEDGMENTS

The authors acknowledge support from the Office of Naval Research (Code No. 331). P.L. and A.P. were supported in part by the San Diego State Foundation Grant No. C-2003-00307.

- 
- [1] V. In, A. Bulsara, A. Palacios, P. Longhini, A. Kho, and J. Neff, *Phys. Rev. E* **68**, 045102(R) (2003).
  - [2] A. Bulsara, C. Seberino, L. Gammaitoni, M. Karlsson, B. Lundqvist, and J. W. C. Robinson, *Phys. Rev. E* **67**, 016120 (2003).
  - [3] V. In, A. Palacios, P. Longhini, J. Neff, and B. Meadows, *Phys. Rev. Lett.* **91**, 244101 (2003).
  - [4] For a good overview, see, e.g., W. Bornhofft and G. Trenkler, in *Sensors, A Comprehensive Survey*, Vols. 1 and 2, edited by W. Gopel, J. Hesse, and J. Zemel (VCH, New York, 1992).
  - [5] E. Doedel and X. Wang, Computer code AUTO94, California Institute of Technology, 1994.
  - [6] See, e.g., H. Stanley, *Introduction to Phase Transitions and Critical Phenomena* (Oxford University Press, Oxford, 1971).
  - [7] J. Acebron, W.-J. Rappel, and A. Bulsara, *Phys. Rev. E* **67**, 016210 (2003).
  - [8] A. Nikhitin, N. Stocks, and A. Bulsara, *Phys. Rev. E* **68**, 036133 (2003).
  - [9] B. Ando, S. Baglio, A. Bulsara, and L. Gammaitoni, in *Proceedings of the IEEE International Symposium on Circuits and Systems, Scottsdale, Arizona, 2003* (IEEE, 2003), Vol. 4, pp. 768–771; B. Ando, S. Baglio, A. Bulsara, and V. Sacco, in *Proceedings of the 24th IEEE Instrumentation and Measurement Conference, Como, Italy, 2004* (IEEE, 2004), p. 1419; and unpublished.
  - [10] M. Inchiosa, V. In, A. Bulsara, K. Wiesenfeld, T. Heath, and M. Choi, *Phys. Rev. E* **63**, 066114 (2001).